Mass transfer from single carbon-dioxide bubbles in surfactant-electrolyte mixed aqueous solutions in vertical pipes

Hori, Yohei
Bothe, Dieter
Hayashi, Kosuke
Hosokawa, Shigeo
Tomiyama, Akio

(Citation)
International Journal of Multiphase Flow,124:103207

(Issue Date)
2020-03

(Resource Type)
journal article

(Version)
Accepted Manuscript

(URL)
https://hdl.handle.net/20.500.14094/90006837

Title: Mass transfer from single carbon-dioxide bubbles in surfactant-electrolyte mixed aqueous solutions in vertical pipes

Authors: Yohei Hori[1], Dieter Bothe[2], Kosuke Hayashi[1], Shigeo Hosokawa[1], Akio Tomiyama[1*]

Affiliation1: Graduate School of Engineering, Kobe University
Address: 1-1 Rokkodai, Nada, Kobe, Hyogo 657-8501, Japan

Affiliation2: Department of Mathematics, TU Darmstadt,
Address: Schlossgartenstraße 7, 64289 Darmstadt, Germany

[*]Corresponding author:

Akio Tomiyama
Professor
Department of Mechanical Engineering
Graduate School of Engineering
Kobe University
Tel. & Fax: +81-78-803-6131
e-mail address: tomiyama@mech.kobe-u.ac.jp

Abstract

Mass transfer from single carbon-dioxide (CO_2) bubbles rising through vertical pipes filled with surfactant–electrolyte mixed aqueous solutions was measured to study the combined effects of surfactant and electrolyte on the mass transfer. Triton X-100 and sodium chloride (NaCl) were used for surfactant and electrolyte, respectively. The surface tension, σ_{eq}, at an equilibrium state decreased with increasing the concentration of NaCl at a constant concentration of Triton X-100. The pipe diameters were 12.5 and 18.2 mm. A wide range of bubble diameter covered various bubble shapes from ellipsoidal to Taylor bubbles. The combined effects of Triton X-100 and NaCl on the Sherwood number, *Sh*, showed a different trend from those of alcohol and electrolyte, i.e. bubbles in the Triton X-100–NaCl mixed aqueous solution were not fully-contaminated even with the same σ_{eq} as in the condition fully-contaminated with Triton X-100, due to the difference in distributions of surfactant concentrations at the interface. The *Sh* of bubbles fully-contaminated with Triton X-100 were not affected by the presence of NaCl. The *Sh* of contaminated Taylor bubbles can be expressed as a combination of functional forms of available *Sh* correlations for clean and fully-contaminated Taylor bubbles.

Keywords: Sodium chloride, Triton X-100, Sherwood number, Surface tension

Nomenclature

A	bubble surface area, m^2
C_A	alcohol concentration, mol/m^3
C_N	NaCl concentration, wt.%
C_S	CO_2 concentration at bubble interface, mol/m^3
C_T	Triton X-100 concentration, mol/m^3
d	bubble diameter, m
d_T	transition bubble diameter, m
d^*	dimensionless bubble diameter
D	pipe diameter, m
D_L	diffusion coefficient, m^2/s
H	Henry constant, Pa
Ha	Hatta number
k_a	adsorption rate constant, $m^3/mol \cdot s$
k_d	desorption rate constant, 1/s
k_L	mass transfer rate, m/s
L	length of Taylor bubble, m
n	mole, mol
P	pressure inside bubble, Pa
Pe_D	Peclet number
R	universal gas constant, J/(K·mol)
Re	bubble Reynolds number, characteristic length: d
Re_D	bubble Reynolds number, characteristic length: D
Sc	Schmidt number
Se	surface coverage ratio
Sh	Sherwood number
Sh_D	modified Sherwood number
V_B	bubble rise velocity, m/s
X	mole fraction in bubble

Greek symbols

Γ	interfacial surfactant concentration, mol/m^2
Γ_{eq}	interfacial surfactant concentration in equilibrium state, mol/m^2
Γ_m	saturated interfacial surfactant concentration, mol/m^2
θ	dimensionless group consisting of sorption properties of surfactant
λ	diameter ratio, $\lambda = d/D$
μ_L	liquid viscosity, Pa·s
ρ_L	liquid density, kg/m^3
σ_{eq}	surface tension, N/m

Subscripts

i	gas component
1	time 1
2	time 2
12	time 12 ($= t_1 + t_2$)

1. Introduction

Impurities dissolving in liquid, e.g. surface-active agents (surfactants) and surface-inactive electrolytes, are known to affect mass transfer rates, k_L, of bubbles in the liquid. Multiphase flows in industrial applications such as sequestration of carbon dioxide (CO_2) in ocean (Kajishima et al, 1997) and chemical reactors (Akita et al., 1973) may include impurities in the liquid phase. A number of studies have therefore been carried out to model the effects of impurities on k_L.

Many studies on the effects of the adsorption-desorption properties of surfactant on k_L have been carried out (Koide et al., 1976; Sardeing et al., 2006; Aoki et al., 2015a, 2017; Haghnegahdar et al., 2016). Sardeing et al. (2006) proposed a k_L model for contaminated bubbles by taking into account the adsorption-desorption kinetics of surfactant and the surface coverage ratio, *Se* ($=\Gamma_{eq}/\Gamma_m$), where Γ_{eq} is the surfactant concentration at bubble interface in an equilibrium state, and Γ_m the saturated interfacial surfactant concentration. Koide et al. (1976) measured k_L of contaminated bubbles using several alcohols, i.e. 1-hexanol, 1-heptanol and 1-octanol, which behave like surfactant. The k_L of bubbles contaminated with alcohol were found to be smaller than those in clean systems. The effect of the presence of alcohol on the reduction in k_L increased with increasing the carbon chain length of alcohol. The k_L of bubbles contaminated with alcohols in vertical pipes were measured in our previous study (Aoki et al. 2017). The k_L of bubbles decreased with increasing the alcohol concentration, C_A, whereas they were independent of C_A at high concentrations, i.e. the bubbles were fully-contaminated from the point of view of mass transfer. The same trend was reported for bubbles contaminated with Triton X-100 in a 12.5 mm pipe (Aoki et al., 2015a, 2015b) and in a 5.96 mm pipe (Haghnegahdar et al., 2016). The authors (Hori et al., 2017) also studied the effects of electrolyte on k_L of single bubbles in vertical pipes using sodium chloride (NaCl) for the electrolyte. The Sherwood numbers, *Sh*, of bubbles in NaCl aqueous solutions were the same as those in clean water, whereas k_L of bubbles decreased with increasing the NaCl concentration, C_N, mainly due to the reduction of the diffusion coefficient of CO_2 in the liquid phase. The presence of the electrolyte is reported to enhance the adsorption of surfactant to the bubble interface (Yekeen et al., 2017) and reduce the surface tension, σ (Xu et al., 2009). Since the bubbles in seawater, in which electrolytes are dissolved, could be contaminated (Olsen et al., 2017), the authors (Hori et al., 2019) studied the combined effects of the surfactant and the electrolyte on k_L using alcohols and NaCl for the surfactant and the electrolyte, respectively. The presence of NaCl enhanced the adsorption of the alcohols to an interface, so that σ decreased with increasing C_N while keeping C_A constant. The Sherwood

numbers were the same when σ were the same and *Sh* were well correlated in terms of the bubble Reynolds number, the Schmidt number, and a bubble–diameter–effect multiplier.

It is well known that the sorption kinetics of Triton X-100 is different from those of alcohols (Takagi et al., 2003; Hayashi and Tomiyama, 2012). Aoki et al. (2015b) pointed out that k_L of Taylor bubbles contaminated with Triton X-100 are largely different from those contaminated with 1-octanol because of the difference in the surfactant distributions at the bubble interfaces. **Fig. 1** shows distributions of Triton X-100 and 1-octanol at the interfaces of Taylor bubbles (Aoki et al., 2015b), where *Ha* is the Hatta number which is the ratio of the adsorption rate to the advection rate and Γ the interfacial surfactant concentration. In the 1-octanol case, *Ha* is large, i.e. $O(10^1)$, so that Γ becomes high in the whole interface of a Taylor bubble, i.e. $\Gamma \approx \Gamma_{eq}$. On the other hand, *Ha* in the Triton X-100 case is much smaller, i.e. $O(10^{-1})$, and therefore, Triton X-100 accumulates only in the tail region of a Taylor bubble and the interface is clean except for the tail region, where $\Gamma \approx \Gamma_m$. Therefore it is speculated that the combined effects of Triton X-100 and NaCl on k_L differ from those of alcohol and NaCl. However no studies have been carried out on the former effect. Hence the combined effects of Triton X-100 and NaCl on k_L of single CO_2 bubbles in vertical pipes were studied in this study. The pipe diameters, *D*, were 12.5 and 18.2 mm. The diameter ratio, λ, which is the ratio of the sphere-volume-equivalent bubble diameter, *d*, to *D* was widely varied to cover various bubble shapes, i.e. ellipsoidal, cap, semi-Taylor and Taylor bubbles. The applicability of k_L correlations to long-term dissolution processes of bubbles in the Triton X-100–NaCl mixed aqueous solutions was examined through comparisons with the data.

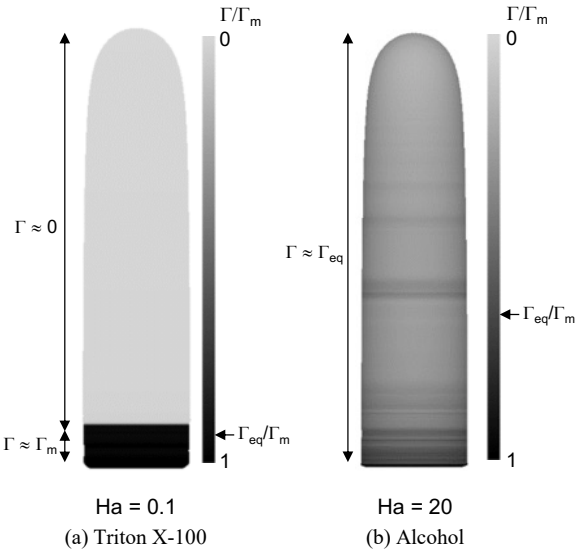

Fig. 1 Distributions of Γ at interfaces of Taylor bubbles of d = 20 mm (Aoki et al., 2015b)

2. Experimental

Fig. 2 shows the experimental setup, which consists of the vertical pipe and the lower and upper tanks. Two pipes of D = 12.5 and 18.2 ± 0.05 mm were used. The pipe length was 2000 mm. The reference elevation (z = 0 mm) was set at 1900 mm below the free surface in the upper tank. The pipe was made of fluorinated-ethylene-propylene (FEP) resin, whose refractive index (1.338) is close to that of water (1.333). The FEP pipe was installed in the acrylic duct. Water was filled in the gap between the duct and the FEP pipe, which enabled observation of bubble images without any optical distortion. Water purified using a Millipore system (Elix 3) and CO_2 of 99.9 vol.% purity were used for the liquid and gas phases, respectively. Triton X-100 (Wako Pure Chemical Industries) and NaCl (99.5 % purity, Wako Pure Chemical Industries) were used for the surfactant and the electrolyte, respectively. The sorption properties of Triton X-100 (Takagi et al., 2003) in the following Langmuir isotherm (Frumkin and Levich, 1947) are k_a = 50 m^3/mol·s, k_d = 0.033 s^{-1}, and $\Gamma_m = 2.9 \times 10^{-6}$ mol/m^2, where k_a is the adsorption rate constant and k_d the desorption rate constant:

$$j = k_a C_A(\Gamma_m - \Gamma_{eq}) - k_d \Gamma_{eq} \tag{1}$$

Here j is the net adsorption flux of surfactant between the liquid phase and the bubble interface.

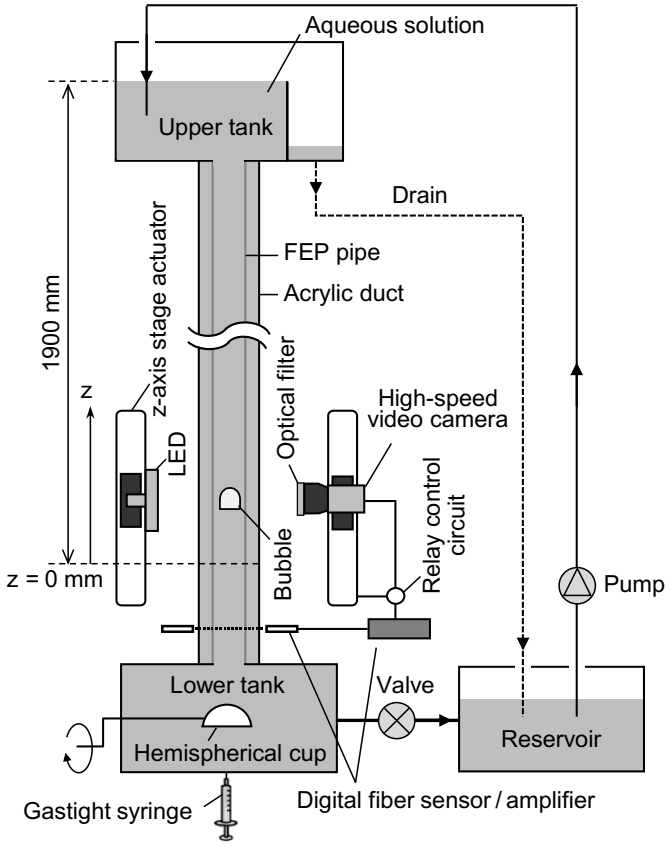

Fig. 2 Experimental setup

Fig. 3 shows σ_{eq} between air and Triton X-100–NaCl mixed aqueous solutions, where C_T is the concentration of Triton X-100 and σ_{eq} the surface tension at an equilibrium state. The σ_{eq} were measured using the pendant bubble method (Pan et al., 1998), in which σ decreases with time due to adsorption of the surfactant until Γ reaches Γ_{eq}, at which $\sigma = \sigma_{eq}$. At constant C_T, σ_{eq} decreases with increasing C_N. The decrease in σ_{eq} implies that Γ_{eq} increases with C_N. The presence of NaCl, therefore, enhances the adsorption of Triton X-100 as in the alcohol cases (Hori et al., 2019). Three combinations of C_T and C_N with the same σ_{eq}, i.e. σ_{eq} = 0.053 N/m, were selected for the experimental condition. The physical properties of the liquid and gas phases are summarized in **Table 1**, where ρ_L is the liquid density, μ_L the liquid viscosity, D_L the diffusion coefficient of CO_2 in NaCl aqueous solutions (Himmelblau, 1964), and C_S the CO_2 concentration at the bubble interface (van Krevelen and Hoftijzer, 1948). The data at C_T = 10 $\times 10^{-3}$ mol/m^3 and C_N = 0 wt.%, for which small bubbles were confirmed to be fully-contaminated from the point of view of mass transfer, were quoted from our previous studies (Aoki et al., 2015a; Aoki, 2017).

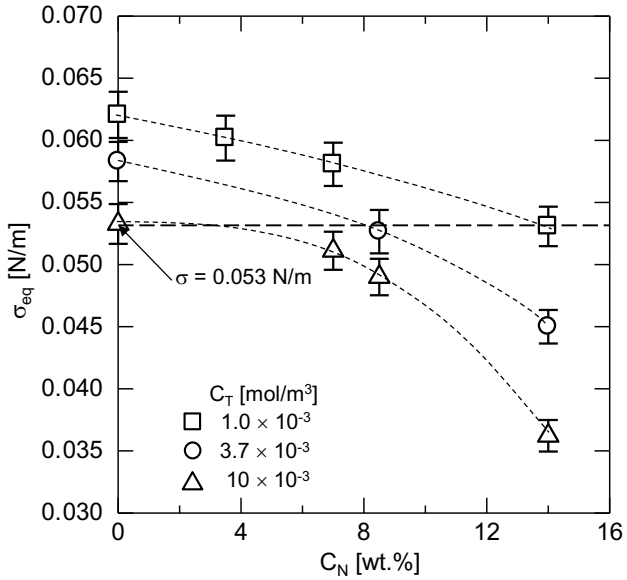

Fig. 3 Surface tension of interface between air and Triton X-100–NaCl mixed aqueous solution

Table 1 Physical properties of liquid and gas phases

C_T [mol/m^3]	1×10^{-3}	3.7×10^{-3}	10×10^{-3}
C_N [wt.%]	14	8.5	0
σ_{eq} [N/m]	0.053	0.053	0.053
ρ_L [kg/m^3]	1095	1057	997
μ_L [Pa·s]	1.17×10^{-3}	1.03×10^{-3}	0.89×10^{-3}
D_L [m^2/s]	1.50×10^{-9}	1.66×10^{-9}	1.90×10^{-9}
C_S [mol/m^3]	19.4	24.5	34.0

Mass transfer rates of bubbles rising through stagnant liquid in the pipes were measured at atmospheric pressure and room temperature (298 ± 1.0 K). The liquid was circulated using the pump before each run to refresh the liquid in the pipe. A predetermined amount of CO_2 gas, whose volume was measured using the gastight syringe, was injected from the bottom of the lower tank and stored in the hemispherical cup. A single bubble was released by rotating the cup. Front and side images of a bubble in the test section were recorded using the two synchronized video cameras (Integrated Design Tool, M3, frame rate: 250 frame/s, exposure time: 1000 μs, spatial resolution: 0.04–0.05 mm/pixel). The green and red LED light sources (NICHIA, NSPG510AS; ROHM, SLI-580UT3F) were used for back illumination. The video cameras and LEDs were mounted on the z-axis actuators (SUS Corp., SA-S6AM) to synchronize their motions. Bubbles were tracked for $0 \le z \le 550$ mm.

An image processing method (Hosoda et al., 2014) was utilized to measure bubble volumes, diameters and positions. The original gray-scale images were transformed into binary images. A three dimensional bubble shape was reconstructed by piling up the elliptic disks by assuming that the horizontal cross sections of a bubble were elliptical. The sphere-volume-equivalent bubble diameters, d, were evaluated from the volume of the reconstructed bubble shapes. The bubble rise velocity, V_B, was obtained as the averaged velocity of a bubble in the test section. With the measurement range of z, V_B could be measured for more than ten periods of the bubble path oscillation. It should be noted that the effects of the mass transfer on V_B were negligibly small since the change in d due to mass transfer was small. Uncertainties estimated at 95% confidence in d and V_B were ± 2.1% and 0.20%, respectively. The d ranged from 5 to 25 mm, and therefore, the ranges of λ (= d/D) were 0.4–1.7 and 0.3–1.4 for D = 12.5 and 18.2 mm, respectively.

The k_L was evaluated from the rate of decrease in d. The change in the moles, n, of CO_2 inside a bubble in an isothermal flow is given by

$$\frac{\mathrm{d}n}{\mathrm{d}t} = -k_L A(C_S - C_0) \tag{2}$$

where t is the time, A (= πd^2) the bubble surface area, and C_0 the CO_2 concentration in the liquid phase. The C_S is given by Henry's law as follows:

$$PX = \frac{C_S}{C_S + C_L} H \tag{3}$$

where P is the pressure inside a bubble, X the mole fraction of CO_2 in a bubble, C_L the H_2O

concentration (55.4 kmol/m^3), and H the Henry constant. By postulating that X is close to unity and $C_0 << C_S$, Eq. (2) can be rewrriten as (Hori et al., 2019)

$$k_L = -\frac{H - P(z)}{\pi d^2 C_L P(z)} \frac{\mathrm{d}n}{\mathrm{d}t} \tag{4}$$

The dn/dt can be expressed in terms of P and d by assuming that CO_2 is an ideal gas:

$$\frac{\mathrm{d}n}{\mathrm{d}t} = \frac{\pi}{6RT} \frac{\mathrm{d}(Pd^3)}{\mathrm{d}t} \tag{5}$$

where R is the universal gas constant. The k_L was calculated by substituting Eq. (5) into Eq. (4) and applying the centered difference between t_1 and t_2 for d(Pd^3)/dt:

$$k_L = \frac{(H - P_{12})(P_2 d_2^3 - P_1 d_1^3)}{6RT(t_2 - t_1) d_{12}^2 C_L P_{12}} \tag{6}$$

where the subscripts, 1, 2 and 12, represent the times, t_1, t_2 (> t_1) and t_{12} (= (t_1 + t_2)/2), respectively. The Sh defined by

$$Sh = \frac{k_L d}{D_L} \tag{7}$$

was calculated from k_L by using d_{12} for d.

Long-term dissolution processes of single bubbles were also measured by keeping the bubble elevation at z = 0 mm in downward flows. The measurement was carried out until the mass transfer from the bubble reached an equilibrium state.

3. Results and Discussion

3.1 Bubble shape and rise velocity

Fig. 4(a) shows examples of **(i)** the images of a clean small bubble, **(ii)** a contaminated small bubble in the Triton X-100 aqueous solution and **(iii)**, **(iv)** contaminated small bubbles in the Triton X-100–NaCl mixed aqueous solutions. They showed wobbling motion. The effect of Triton X-100 on the bubble shape is clearly seen in the figure, i.e. capillary waves are formed at the interface of the clean small bubble whereas they are attenuated in the contaminated systems. The effects of the combination of C_T and C_N on the shapes of the small bubbles are small. **Fig. 4(b)** shows examples of the clean and contaminated Taylor bubbles. Capillary waves are formed in the tail region of the clean Taylor bubble, whereas they disappeared in the contaminated systems. **Fig. 5** shows a comparison between the measured lengths, L, of the Taylor bubbles (the axial distance between the nose and the tail) and the following L/D correlation for Taylor bubbles in clean water (Nakahara et al., 2003):

$$\frac{L}{D} = (0.586 - 0.216\lambda + 0.844\lambda^2)\lambda \tag{8}$$

The effects of C_T and C_N on L/D are very small and Eq. (8) well evaluates L/D for all the cases.

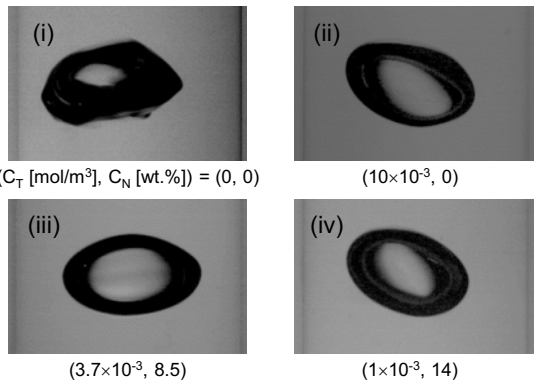

(a) Small bubbles (d = 6 mm, D = 12.5 mm)

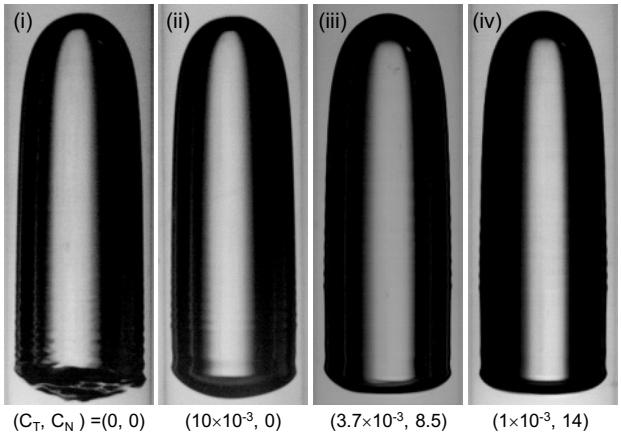

(b) Taylor bubbles (d = 16 mm, D = 12.5 mm)

Fig. 4 Bubble shapes (z = 0 mm)

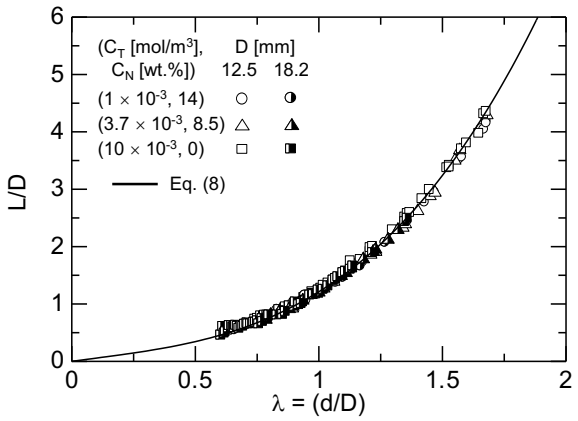

Fig. 5 Comparison between measured L/D and Eq. (8)

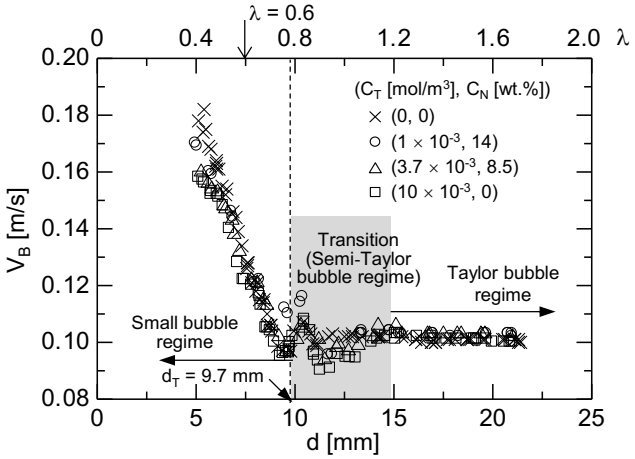

(a) D = 12.5 mm

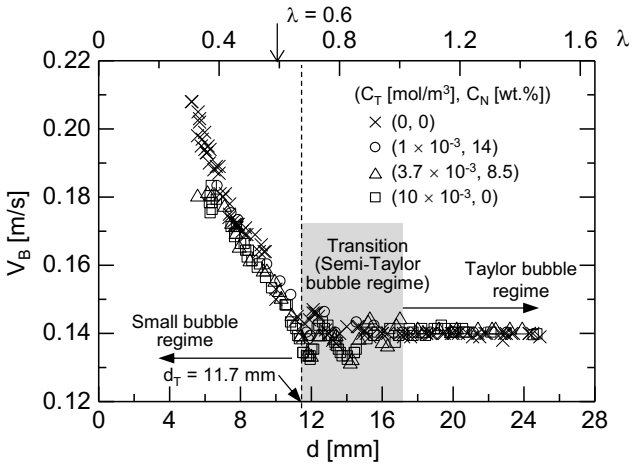

(b) D = 18.2 mm

Fig. 6 Bubble rise velocities

The V_B are shown in **Fig. 6**, in which the data are classified into three regimes, the small (ellipsoidal and cap) bubble regime, the transition (semi-Taylor bubble) regime and the Taylor bubble regime. The V_B of the small bubbles decreases with increasing d due to the increase in the effect of the pipe wall. The d_T in the figure is the bubble diameter at the transition from the small bubble regime to the transition regime (Aoki et al., 2015b), which is defined as the bubble diameter for the abrupt change in the trend of V_B. In the transition regime, the characteristic length governing V_B changes from d to D, and V_B shows complex dependence on d. The effect of the presence of the impurities on V_B is seen for $\lambda < 0.6$, i.e. V_B of contaminated bubbles are lower than those of clean bubbles due to the Marangoni effect (Kurimoto et al., 2013). The combined effects on V_B of contaminated small bubbles are small for $0.6 < \lambda < d/d_T$. This is because the inertial force governs the bubble motion for bubbles in this range of d. In other words, the role played by the surface tension in V_B becomes small in this range (Aoki et al., 2015a). The Taylor bubble regime can be clearly identified since V_B is independent on d. In the Taylor bubble regime, the effects of C_T and C_N on V_B are small.

3.2 Mass transfer rate and Sherwood number

Fig. 7 shows k_L of clean and contaminated bubbles. The k_L of contaminated small bubbles are much lower than those of clean bubbles whereas k_L of contaminated Taylor bubbles asymptotically approach those of clean Taylor bubbles. The decrease rate of k_L of contaminated small bubbles depends on the combination of C_T and C_N even at the same σ_{eq}.

In our previous study (Hori et al., 2019), the authors correlated *Sh* of fully-contaminated small bubbles in alcohol–NaCl mixed aqueous solutions of the same σ_{eq} in the following functional form:

$$Sh = F(d^*)Re^{1/2}Sc^{1/3} \quad \text{for } d^* \le 1.2 \tag{9}$$

where d^* is the dimensionless bubble diameter, $F(d^*)$ a function of d^*, *Re* the bubble Reynolds number and *Sc* the Schmidt number defined by

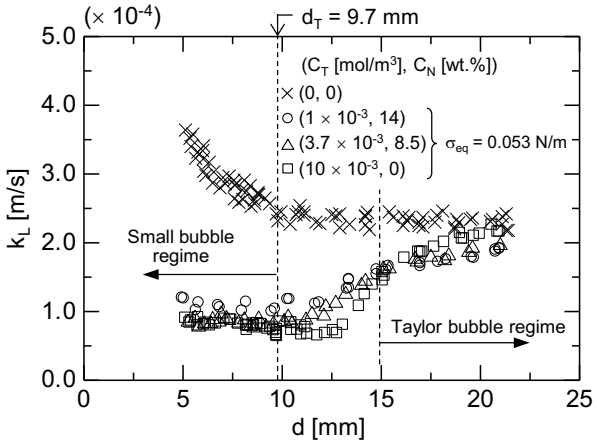

(a) D = 12.5 mm

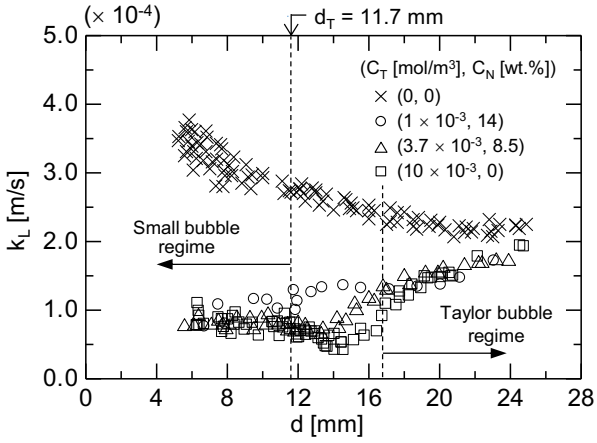

(b) D = 18.2 mm

Fig. 7 Mass transfer rates

$$d^* = d / d_T \tag{10}$$

$$Re = \frac{\rho_L V_B d}{\mu_L} \tag{11}$$

$$Sc = \frac{\mu_L}{\rho_L D_L} \tag{12}$$

The $Sh/(Re^{1/2}Sc^{1/3})$ are plotted against d^* in **Fig. 8**. The data of $C_T = 1 \times 10^{-3}$ mol/m^3 and $C_N = 14$ wt.% for $L/D \leq 1.8$ are higher than the others, i.e. the combined effect of the former is much smaller than those of the latter. These characteristics of Sh are different from those in the 1-octanol–NaCl mixed aqueous solutions (Hori et al., 2019), i.e. Sh of small bubbles in the 1-octanol–NaCl mixed aqueous solutions do not depend on the combination of C_A and C_N if σ_{eq} is the same. The data clearly show that small bubbles in the Triton X-100–NaCl mixed aqueous solutions for $C_T \leq 3.7 \times 10^{-3}$ mol/m^3 were not fully-contaminated from the point of view of mass transfer even in the same σ_{eq} as in the fully-contaminated system ($C_T = 10 \times 10^{-3}$ mol/m^3, $C_N = 0$ wt.%). As is well known, adsorption of surfactant on bubble surface attenuates the capillary waves on small bubble surface, which mitigates surface renewal and as a result k_L decreases. The increase in C_T increases the ratio of the contaminated interface region to the whole bubble surface area, resulted in the decrease of k_L with increasing C_T. The k_L at (C_T, C_N) = (1.0×10^{-3}, 14) larger than that at (10×10^{-3}, 0) implies that Γ in the contaminated region is close to Γ_m and the combined effect is very small there.

As described in the introduction, the interface of a Taylor bubble is clean except for the tail region in the Triton X-100 case (Aoki et al., 2015a). Hence the combination of Triton X-100 and NaCl does not affect the mass transfer in the upper part of a bubble. There is no combined effect of Triton X-100 and NaCl in the tail region of the bubble, since Γ is already close to Γ_m in the tail region. Therefore all the data for $L/D > 1.8$ lie on a single curve.

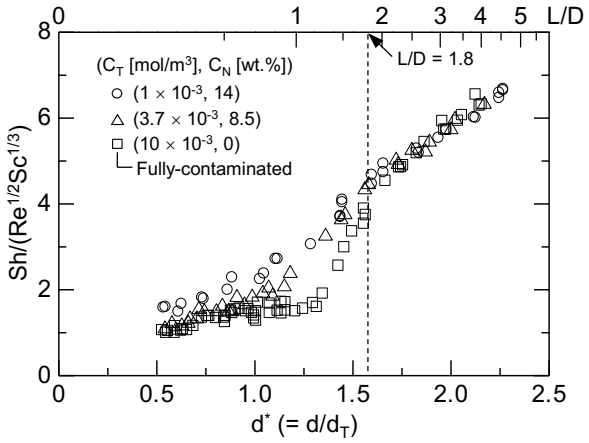

(a) D = 12.5 mm

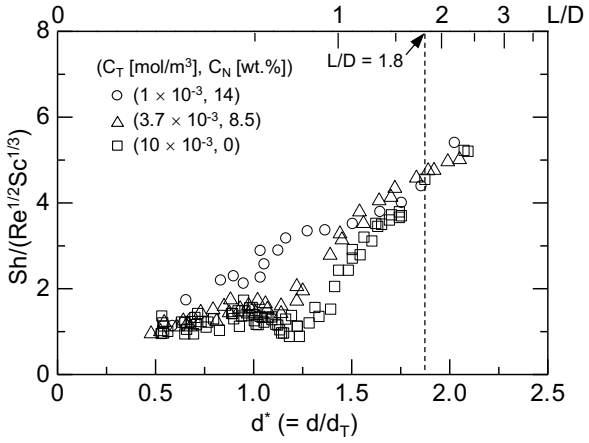

(b) D = 18.2 mm

Fig. 8 $Sh/(Re^{1/2}Sc^{1/3})$ vs. d^*

3.3 Sherwood number in fully-contaminated conditions

Bubbles in C_T = 10 × 10^{-3} mol/m^3 and C_N = 7.0 and 14 wt.% were measured to study the combined effect on *Sh* of fully-contaminated bubbles. As shown in **Fig. 3**, σ_{eq} decreases with increasing C_N while keeping C_T = 10 × 10^{-3} mol/m^3 due to the combined effect. The physical properties in the three conditions, i.e. C_T = 10 × 10^{-3} mol/m^3 and C_N = 0, 7.0 and 14 wt.%, are summarized in **Table 2**. The $Sh/(Re^{1/2}Sc^{1/3})$ in the three conditions are shown in **Fig. 9**. All the data are collapsed onto a single curve. This clearly shows that *Sh* of bubbles fully-contaminated with Triton X-100 are not affected by the presence of NaCl.

Since Aoki et al. (2015b) pointed out that *Sh* of small bubbles fully-contaminated with Triton X-100 are almost the same as those with 1-octanol, the following $F(d^*)$ for small bubbles of $d^* \leq 1.2$ contaminated with 1-octanol (Hori et al., 2019) in Eq. (9) is expected to correlate the present data:

$$F(d^*) = -0.10d^{*2} + 0.88d^* + 0.6 \tag{13}$$

As shown in **Fig. 9**, Eq. (9) with Eq. (13) reasonably evaluates *Sh* of fully-contaminated small bubbles in the Triton X-100–NaCl mixed aqueous solutions. **Fig. 10** compares Eqs. (9) and (13) with the data for $d^* \leq 1.2$. 83% of the data are to within ± 20% errors.

Table 2 Physical properties of liquid and gas phases in fully-contaminated conditions

C_T [mol/m^3]	10 × 10^{-3}	10 × 10^{-3}	10 × 10^{-3}
C_N [wt.%]	0	7.0	14
σ_{eq} [N/m]	0.053	0.051	0.036
ρ_L [kg/m^3]	997	1051	1095
μ_L [Pa·s]	0.89 × 10^{-3}	1.00 × 10^{-3}	1.17 × 10^{-3}
D_L [m^2/s]	1.90 × 10^{-9}	1.71 × 10^{-9}	1.50 × 10^{-9}
C_S [mol/m^3]	34.0	26.0	19.4

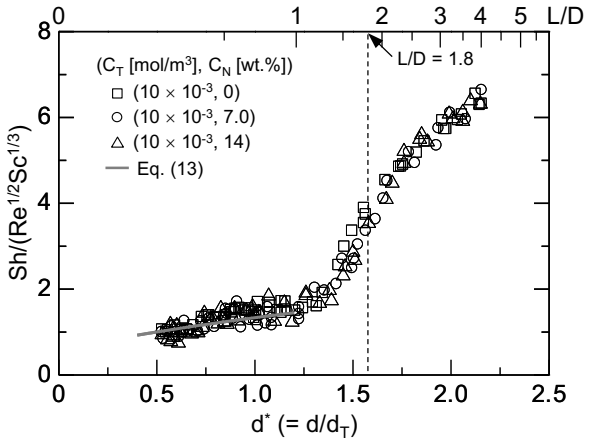

(a) D = 12.5 mm

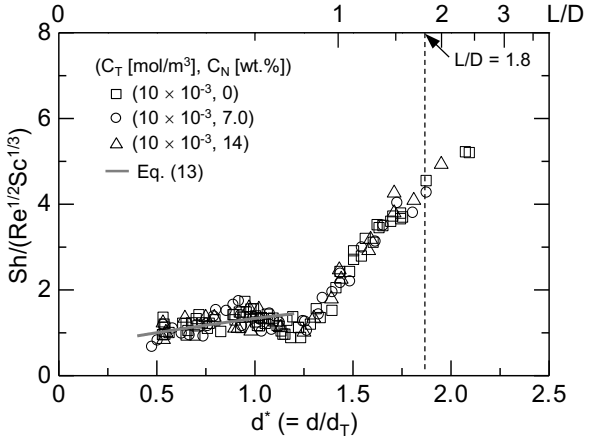

(b) D = 18.2 mm

Fig. 9 $Sh/(Re^{1/2}Sc^{1/3})$ of fully-contaminated bubbles

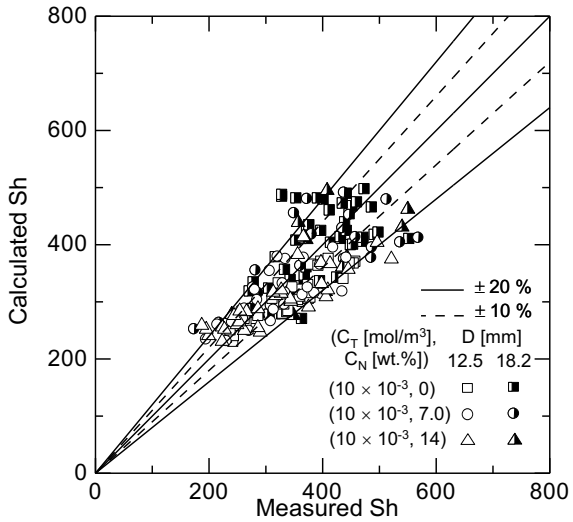

Fig. 10 Comparisons between Eq. (9) with Eq. (13) and data for $d^* \leq 1.2$

The authors (Hori et al., 2019) proposed the following Sherwood number correlation for Taylor bubbles in alcohol–NaCl mixed aqueous solutions:

$$Sh_D = G\left(L/d_T, \theta\right) Re_D^{1/2} Sc^{1/3} \tag{14}$$

where G is a function to take into account the bubble size and surfactant properties, Sh_D the modified Sherwood number, Re_D the modified bubble Reynolds number, and θ a dimensionless group consisting of sorption properties of surfactant. They are defined by

$$Sh_D = \frac{k_L A}{D_L D} \tag{15}$$

$$Re_D = \frac{\rho_L V_B D}{\mu_L} \tag{16}$$

$$\theta = \frac{k_a \Gamma_m}{k_d d_T} \tag{17}$$

In **Fig. 11**, $Sh_D/(Re_D^{1/2} Sc^{1/3})$ are plotted against L/d_T. The data are collapsed onto a single curve, and therefore, Sh_D of Taylor bubbles fully-contaminated with Triton X-100 can be expressed with the functional form of Eq. (14). The following empirical correlation of $G(L/d_T, \theta)$ for alcohol–NaCl mixed aqueous solutions (Hori et al., 2019) is also plotted in the figure:

$$G(L/d_T, \theta) = A(\theta)(L/d_T)^2 + B(\theta)(L/d_T) + C \tag{18}$$

where

$$A(\theta) = -5.6 \times 10^{-5} \theta^{-1.2} \tag{19}$$

$$B(\theta) = 2.8 \theta^{-0.19} \tag{20}$$

$$C = -7.0 \tag{21}$$

As clearly shown, Eq. (14) with Eq. (18) largely underestimates the data. As Aoki et al. (2015b) pointed out, Sherwood numbers of Taylor bubbles contaminated with Triton X-100 and those with 1-octanol have different trends due to the difference in the distributions of Γ in the nose and side regions of the bubbles. Eq. (14) does not take into account this difference and G should be tuned for the Triton X-100 cases. Here G is rewritten as $G(L/d_T)$ and modified for the Triton X-100 case:

$$Sh_D = G\left(L/d_T\right) Re_D^{1/2} Sc^{1/3} \tag{22}$$

$$G(L/d_T) = -0.24(L/d_T)^2 + 11.4(L/d_T) - 11.9 \tag{23}$$

Fig. 12 shows comparisons between Eq. (22) with Eq. (23) and the data. 87% of the data are to within ± 20% errors.

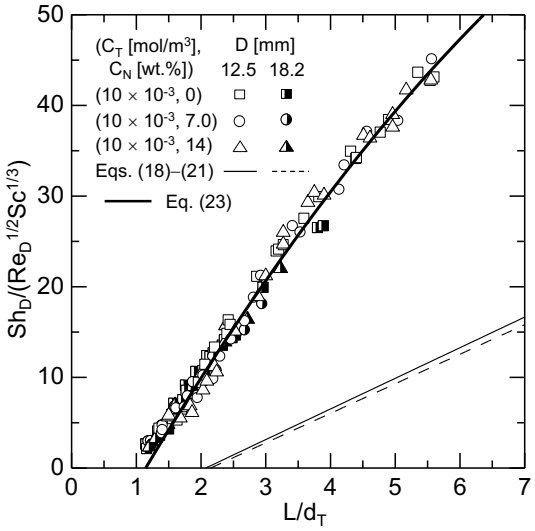

Fig. 11 $Sh_D/(Re_D^{1/2}Sc^{1/3})$ vs. L/d_T

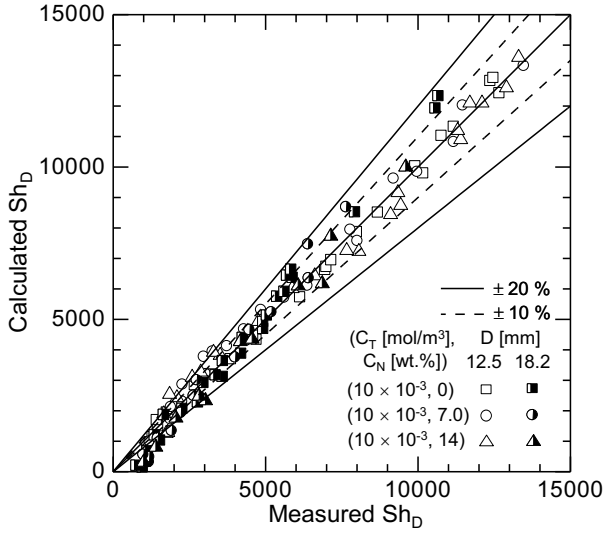

Fig. 12 Comparisons between Eq. (22) with Eq. (23) and data for $d^* > 1.2$

However, the functional form of Eq. (22) does not express the fact that Triton X-100 accumulates only in the tail region of a Taylor bubble, i.e. most of the interface of the Taylor bubble is clean. Hence Sh_D of Taylor bubbles of large d should be expressed with a functional form for clean Taylor bubbles. The Sh_D of clean Taylor bubbles are expressed as (Filla, 1981):

$$Sh_D = f(L/D)\,Pe_D^{1/2} \tag{24}$$

where Pe_D is the Peclet number defined by

$$Pe_D = \frac{V_B D}{D_L} \tag{25}$$

The $Sh_D/Pe_D^{1/2}$ are plotted against L/D in **Fig. 13**. As expected, $Sh_D/Pe_D^{1/2}$ for large bubbles (L/D > 2.5) is well correlated with L/D and $f(L/D)$ in Eq. (24) is given by

$$f(L/D)=3.7\,L/D-0.9 \tag{26}$$

as shown in **Fig. 13**. The Sh_D in intermediate d are expected to be expressed as a combination of Sh_D correlation for fully-contaminated bubbles and that for clean bubbles. Sardeing et al. (2006) proposed the following empirical k_L correlation for contaminated small bubbles which takes into account Se:

$$k_L = Sek_{LR} + (1-Se)k_{LC} \tag{27}$$

where k_{LR} is the mass transfer rate for contaminated interface, k_{LC} the mass transfer rate for clean interface. Since Se (= Γ_{eq}/Γ_m) assumes an equilibrium state, it does not take into account the distribution of the surfactant. As shown in **Fig. 7**, k_L of bubbles contaminated with Triton X-100 (C_T = 10 × 10^{-3} mol/m^3, C_N = 0 wt.%) show almost the same value as those of clean bubbles at d = 21 and 25 mm for D = 12.5 and 18.2 mm, respectively, i.e. d^* ≈ 2.1 for all D. Hence Se is expected to be expressed as a function of d^*. Substituting Eqs. (15), (22) and (24) into Eq. (27) yields:

$$Sh_D = \left[Se(d^*)G(L/d_T)Re_D^{1/2}\,Sc^{1/3} \right] + \left[\left\{1-Se(d^*)\right\} f(L/D)\,Pe_D^{1/2} \right] \tag{28}$$

where $Se(d^*)$ is fitted so as to express the fact that the clean interface part increases with increasing d^*:

$$Se(d^*)=-\frac{1}{2}\tanh(11.7d^*-19.8)+\frac{1}{2} \tag{29}$$

Eq. (29) takes into account the fact that Sh_D is for contaminated bubbles when d^* is small and for clean bubbles when d^* >> 1. The $G(L/d_T)$ in Eq. (28) was fitted to the data in the intermediate d, i.e. d^* > 1.2 and L/d_T < 3.5:

$$G(L/d_T)=8.5\,L/d_T-8.0 \tag{30}$$

Fig. 14 shows comparisons between Eqs. (26), (28)–(30) and the data. 96% of the data are to within ± 20% errors.

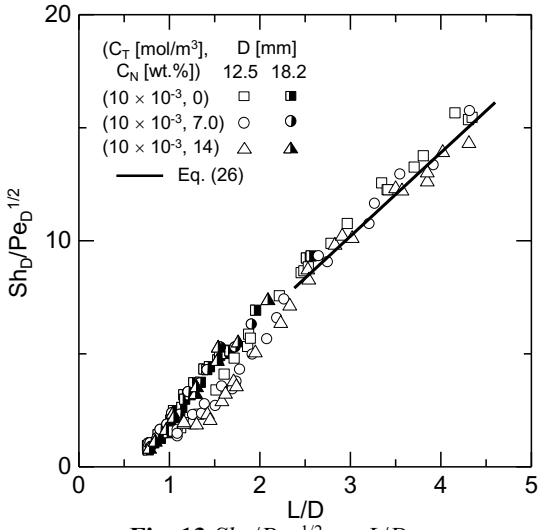

Fig. 13 $Sh_D/Pe_D^{1/2}$ vs. L/D

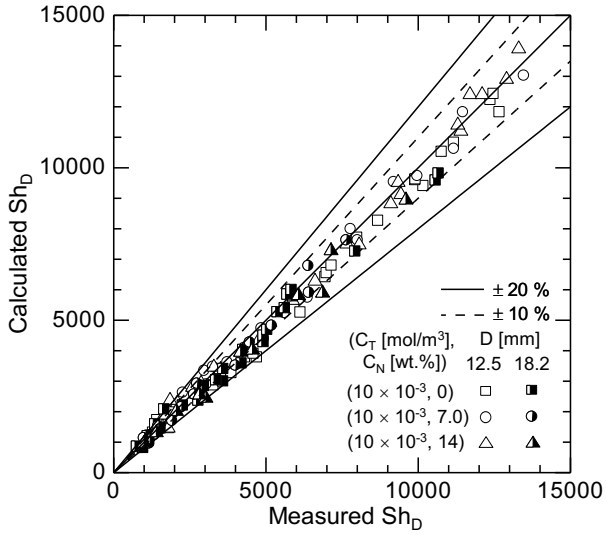

Fig. 14 Comparisons between Eqs. (26), (28)–(30) and data for $d^* > 1.2$

3.4 Long-term dissolution process of fully-contaminated bubble

Bubble diameter changes at $C_T = 10 \times 10^{-3}$ mol/m^3 and $C_N = 7.0$ wt.% are shown in **Fig. 15**. The initial bubble diameter, d_{in}, at $t = 0$ s was 26.7 mm and the initial CO_2 mole fractions, X_{CO2}, were 0.999, 0.8 and 0.5, respectively, where t is the time elapsed from the injection of CO_2 into the hemispherical cup in the lower tank. The time, τ, in the figure is the time elapsed from the bubble arrival at $z = 0$ mm. The bubble diameter decreases due to dissolution, and then, it becomes constant for $\tau > 250$ s. This means that the mass transfer has reached its equilibrium state. The bubble dissolution process was numerically predicted using the Sherwood number correlations. The numerical method (Hosoda et al., 2014) is as follows. The conservation of the number of moles, n_i, of the component i in the gas phase is given by

$$\frac{\mathrm{d}n_i}{\mathrm{d}t} = -\pi d^2 k_{Li}(C_{Si} - C_{0i}) \tag{31}$$

The mass transfer of nitrogen (N_2) and oxygen (O_2) from the liquid phase to the gas phase is not negligible in the bubble dissolution process (Hosoda et al., 2014) since the experimental setup was open to the atmosphere. Hence Eq. (31) was solved for three gas components, i.e. CO_2, N_2 and O_2. The physical properties of these gases for the NaCl aqueous solution of $C_N = 7.0$ wt. % are summarized in **Table 3**, where the molar concentrations, C_0, in the liquid phase were calculated by assuming the equilibrium with the atmosphere. No effect of Triton X-100 on these properties was assumed since C_T [wt.%] was very low, i.e. $C_T < O(10^{-4})$. Therefore the values for the NaCl aqueous solution of $C_N = 7.0$ wt. % were used for the present predictions. When the bubble is kept at the elevation of $z = 0$ mm, the molar concentrations, C_{Si}, at the bubble interface are given by

$$C_{Si} = \frac{C_L P(0) X_i}{H_i - P(0) X_i} \tag{32}$$

where X_i is the mole fraction of the component i:

$$X_i = \frac{n_i}{\sum_{i=1}^{N} n_i} \tag{33}$$

where N is the total number of gas components, i.e. $N = 3$. The mass transfer rates, k_{Li}, were evaluated by using Eqs. (9), (13), (26), (28)-(30) in which V_B was calculated using available correlation (Nakahara et al., 2003) as described in Appendix. The bubble diameter can be expressed in terms of n_i by using the equation of state for an ideal gas:

$$d = \left[\frac{6}{\pi} \left(\sum_{i=1}^{N} \frac{n_i RT}{P(0)} \right) \right]^{1/3} \tag{34}$$

The predicted d are shown in **Fig. 15**. The predictions agree well with all the data. Hence the correlations are applicable to the long-term dissolution processes of fully-contaminated bubbles in the Triton X-100–NaCl mixed aqueous solutions at any initial CO_2 concentrations.

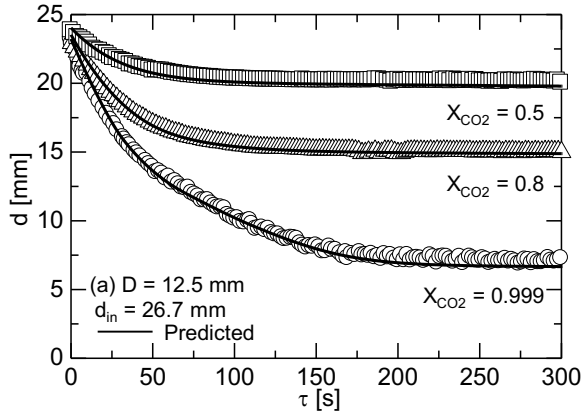

(a) D = 12.5 mm

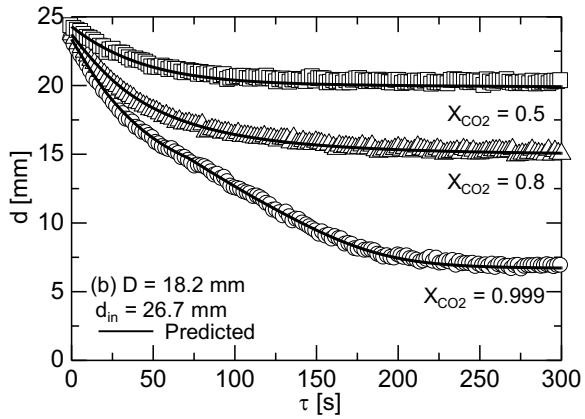

(b) D = 18.2 mm

Fig. 15 Long-term bubble dissolution processes of bubbles in Triton X-100–NaCl mixed aqueous solution (C_T = 10 × 10^{-3} mol/m^3, C_N = 7.0 wt.%)

Table 3 Physical properties of gases in NaCl aqueous solution of C_N = 7.0 wt.% at T = 298 K (Hori et al., 2017)

	CO_2	N_2	O_2
H [GPa]	0.127	5.80	3.26
C_S [mol/m^3]	26	0.45	0.96
D_L [m^2/s]	1.71×10^{-9}	1.80×10^{-9}	2.07×10^{-9}
C_0 [mol/m^3]	0.008	0.35	0.20

4. Conclusions

Combined effects of surfactant and electrolyte on mass transfer from single carbon-dioxide bubbles in vertical pipes were studied. Triton X-100 and sodium chloride (NaCl) were used for the surfactant and the electrolyte, respectively. Various combinations of the Triton X-100 concentrations and the NaCl concentrations were selected for the experimental conditions. The pipe diameters, D, were 12.5 and 18.2 mm. The bubble diameter, d, was varied to cover ellipsoidal to Taylor bubbles. The mass transfer rates, k_L, were evaluated from the rate of change in d and the Sherwood numbers, Sh, were calculated from k_L. Long-term dissolution processes of single bubbles in the Triton X-100–NaCl mixed aqueous solutions were measured to examine the applicability of Sherwood number correlations. The following conclusions were obtained in the present experimental condition:

(1) The combined effects of Triton X-100 and NaCl on Sh showed a different trend from those of alcohol and electrolyte, i.e. bubbles in Triton X-100-NaCl mixed aqueous solution were not fully-contaminated even in the same surface tension as in the condition fully-contaminated with Triton X-100, due to the difference in the distribution of surfactant concentration at the interface.

(2) The Sh of bubbles fully-contaminated with Triton X-100 are not affected by the presence of NaCl.

(3) The modified Sherwood numbers, Sh_D, of Taylor bubbles fully-contaminated with Triton X-100 can be expressed as a combination of the functional forms of available Sh_D correlations for clean and fully-contaminated Taylor bubbles.

(4) The Sherwood number correlations, Eqs. (9) and (28), give good predictions for long-term dissolution processes of fully-contaminated bubbles in Triton X-100–NaCl mixed aqueous solutions.

Appendix A

Fig. A1 compares the V_B data in **(a), (b)** the fully-contaminated conditions and **(c)** the intermediately-contaminated condition with the following empirical correlation for single clean bubbles in vertical pipes (Nakahara et al., 2003):

$$V_B = \max[V_{BS}, V_{BT}] \tag{A1}$$

where V_{BS} and V_{BT} are the terminal velocities of small and Taylor bubbles, respectively. They are defined by

$$V_{BS} = \phi(\lambda)^{-1/2} V_{B0} \tag{A2}$$

$$V_{BT} = Fr\sqrt{\frac{(\rho_L - \rho_G)gD}{\rho_L}} \tag{A3}$$

where $\phi(\lambda)$ is the wall effect multiplier, V_{B0} the terminal velocity of a bubble in an infinite stagnant liquid, Fr the Froude number, and ρ_G the gas density. The $\phi(\lambda)$ is given by

$$\phi(\lambda) = \max[1, 4((1-\lambda^2)^{1.5} + 1.13e^{-\lambda})^{-2}] \tag{A4}$$

where the first and second terms in the right hand side of Eq. (A4) are the wall effect multipliers for ellipsoidal bubbles (Clift et al., 1978) and for cap bubbles (Wallis, 1964), respectively. The V_{B0} is given by the balance of the drag force and the buoyancy, i.e.

$$V_{B0} = \sqrt{\frac{4(\rho_L - \rho_G)gd}{3C_D\rho_L}} \tag{A5}$$

where C_D is the drag coefficient given by (Tomiyama et al., 1998)

$$C_D = \max\left[\min\left[\frac{16}{Re}(1+0.15Re^{0.687}), \frac{48}{Re}\right], \frac{8}{3}\frac{Eo}{Eo+4}\right] \tag{A6}$$

where Eo is the Eötvös number defined by

$$Eo = \frac{(\rho_L - \rho_G)gd^2}{\sigma} \tag{A7}$$

The σ_{eq} shown in **Table 1** were used for σ to evaluate Eo. The Fr is evaluated by using the following correlation (Kurimoto et al., 2013):

$$Fr = \sqrt{\frac{\beta \cdot \gamma}{\frac{\gamma}{0.35^2} + \alpha}} \tag{A8}$$

$$\alpha = \frac{1}{Re_D}\left(1 - 0.05\sqrt{Re_D}\right)$$

$$\beta = \left(1 + \frac{3.87}{Eo_D^{1.68}}\right)^{-18.4}$$

$$\gamma = 0.0025(3 + \beta)$$

where Re_D is the modified bubble Reynolds number and Eo_D the Eötvös number defined by

$$Re_D = \frac{\rho_L V_B D}{\mu_L} \tag{A9}$$

$$Eo_D = \frac{(\rho_L - \rho_G) g D^2}{\sigma} \tag{A10}$$

respectively. Here the surface tension in a clean system, i.e. σ = 0.072 N/m, was used to evaluate Eo_D since Aoki et al. (2015a) pointed out that the nose region of a Taylor bubble contaminated with Triton X-100 is almost clean even in the fully-contaminated system. Eq. (A1) agrees well with the data not only in the small bubble regime but also in the Taylor bubble regime for fully-contaminated conditions as shown in **Fig. A1(a) and (b)**. This result proves that the nose regions of the Taylor bubbles in Triton X-100–NaCl mixed aqueous solutions are clean even in the fully-contaminated condition. Eq. (A1) was, therefore, used in numerical predictions of the long-term dissolution processes of fully-contaminated bubbles in Sec. 3.4. On the other hand, Eq. (A1) slightly underrates V_B of intermediately-contaminated small bubbles as shown in **Fig. A1(c)**, which proves that the bubbles were not fully-contaminated even in the same σ_{eq} as the fully-contaminated condition, i.e. $\sigma_{eq} \approx 0.053$ N/m.

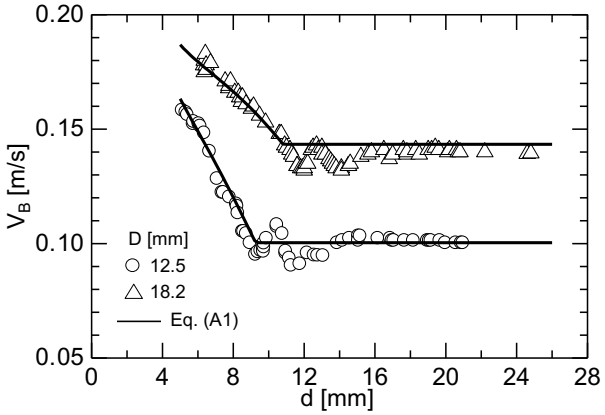

(a) (C_T [mol/m^3], C_N [wt.%]) = (10×10^{-3}, 0)

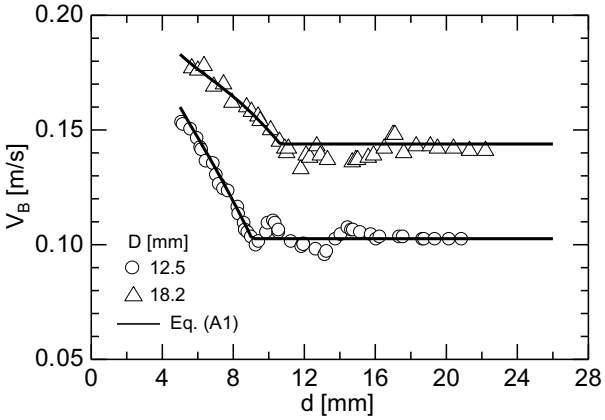

(b) (10×10^{-3}, 7.0)

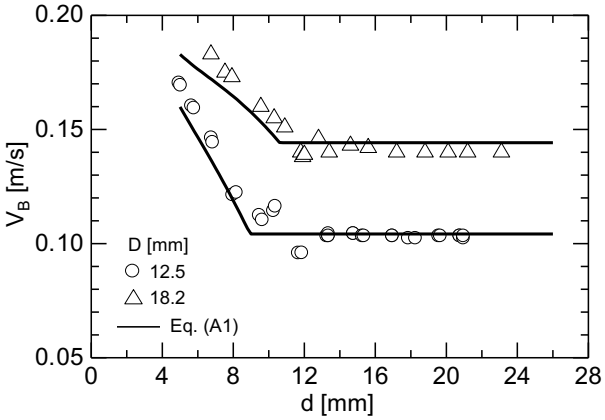

(c) (1×10^{-3}, 14)

Fig. A1 Comparisons between Eq. (A1) and data

Acknowledgment

The authors would like to express their thanks to Mr. Yutaka Hirota for his assistance in this work and the financial support by JSPS KAKENHI Grant Number 18H03756.

References

Akita, K., Yoshida, F., Gas holdup and volumetric mass transfer coefficient in bubble columns, Ind. Eng. Chem. Process Des. Develop. 12 (1973) 76−80.

Aoki, J., Hayashi, K., Tomiyama, A., Mass transfer from single carbon dioxide bubbles in contaminated water in a vertical pipe, Int. J. Heat Mass Transfer. 83 (2015a) 652–658.

Aoki, J., Hayashi, K., Hosokawa, S., Tomiyama, A., Effects of surfactant on mass transfer from single carbon dioxide bubbles in vertical pipes, Chem. Eng. Tech., 38 (11) (2015b) 1955−1964.

Aoki, J., Hori, Y., Hayashi, K., Hosokawa, S., Tomiyama, A., Mass transfer from single carbon dioxide bubbles in alcohol aqueous solutions in vertical pipes, Int. J. Heat Mass Transfer, 108 (2017) 1991−2001.

Aoki, J., PhD thesis, Kobe University, Kobe, Japan, (2017).

Clift, R., Grace, J.R., Weber, M.E., Bubbles, Drops, and Particles, Academic Press, New York, U.S.A. (1978).

Filla, M., Gas absorption from a slug held stationary in downflowing liquid, Chem. Eng. J. 22 (1981) 213–220.

Frumkin, A., Levich, V.G., On surfactants and interfacial motion, Zh. Fiz. Khim. 21 (1947) 1183–1204.

Haghnegahdar, M., Beden, S., Hampel, U., Investigation of surfactant effect on the bubble shape and mass transfer in a milli-channel using high-resolution microfocus X-ray imaging, Int. J. Multiphase Flow 87 (2016) 184−196.

Hayashi, K., Tomiyama, A., Effects of surfactant on terminal velocity of a Taylor bubble in a vertical pipe, Int. J. Multiphase Flow 39 (2012) 78−87.

Himmelblau, D.M., Diffusion of dissolved gases in liquid, Chem. Rev. 64 (1964) 527−545.

Hori, Y., Hayashi, K., Hosokawa, S., Tomiyama, A., Mass transfer from single carbon-dioxide bubbles in electrolyte aqueous solutions in vertical pipes, Int. J. Heat Mass Transfer, 111 (2017) 663−671.

Hori, Y., Hirota, Y., Hayashi, K., Hosokawa, S., Tomiyama, A., Combined effects of alcohol and electrolyte on mass transfer from single carbon-dioxide bubbles in vertical pipes, Int. J. Heat Mass Transfer, 136 (2019) 521−530.

Hosoda, S., Abe, S., Hosokawa, S., Tomiyama, A., Mass transfer from a bubble in a vertical pipe, Int. J. Heat Mass Transfer, 69 (2014) 215–222.

Kajishima, T., Saito, T., Nagaosa, R., Kosugi, S., GLAD: a gas-lift method for CO_2 disposal into the ocean, Energy, 22 (1997) 257–262.

Koide, K., Hayashi, T., Sumino, K., Iwamoto, S., Mass transfer from single bubbles in aqueous solutions of surfactants, Chem. Eng. Sci. 31 (1976) 471–484.

Kurimoto, R., Hayashi, K., Tomiyama, A., Terminal velocities of clean and fully-contaminated drops in vertical pipes, Int. J. Multiphase Flow 49 (2013) 8–23.

Nakahara, Y., Tomiyama, A., Shapes and rising velocities of single bubbles in vertical pipes, Trans. Jpn. Soc. Mech. Eng. B 69 (685) (2003) 2001−2009.

Olsen, J.E., Dunnebier, D., Davies, E., Skjetne, P., Morud, J., Mass transfer between bubbles and seawater, Chem. Eng. Sci., 161 (2017) 308−315.

Pan, R., Green, J., Maldarelli, C., Theory and experiment on the measurement of kinetic rate constants for surfactant exchange at an air/water interface, J. Colloid Interface Sci., 205 (1998) 213−230.

Sardeing, R., Painmanakul, P., Hébrard, G., Effect of surfactants on liquid-side mass transfer coefficients in gas–liquid systems: a first step to modeling, Chem. Eng. Sci. 61 (19) (2006) 6249–6260.

Takagi, S., Uda, T., Watanabe, Y., Matsumoto, Y., Behavior of a rising bubble in water with surfactant dissolution, Trans. Jpn. Soc. Mech. Eng. Ser. B 69 (686) (2003) 2192–2199.

Tomiyama, A., Kataoka, I., Zun, I., Sakaguchi, T., Drag coefficient of single bubbles under normal and micro gravity conditions, JSME Int J., B 41 (2) (1998) 472–479.

van Krevelen, D.W., Hoftijzer, P.J., Sur la solubilite des gaz dans les solutions aqueouses, Ind. 21st Congr. Int. Chim. Ind. (1948) 168.

Wallis, G.B., One-Dimensional Two-Phase Flow, McGraw- Hill, (1964).

Xu, Q., Nakajima, M., Ichikawa, S., Nakamura, N., Roy, P., Okadome, H., Shiina, T., Effects of surfactant and electrolyte concentrations on bubble formation and stabilization, J. Colloid Interface Sci. 332 (2009) 208−214.

Yekeen, N., Manan, M.A., Idris, A.K., Samin, A.M., Influence of surfactant and electrolyte concentrations on surfactant adsorption and foaming characteristics, J. Petro. Sci. Eng. 149 (2017) 612−622.